Journal of Environment and Earth Science
ISSN 2224-3216 (Paper) ISSN 2225-0948 (Online)
Vol.15, No.2, 2025

Efficient Removal of Crystal Violet Using Fly Ash Steel Slag Based Geopolymer

Hossain Md Elias[1*] Ling Xiao[1] Sun Shushuang[1] Wadjou Christian[1] Ahmed Md. Syekat[1] Ahmed Tanvir[1] Zhang Lingling[1]

1. School of Energy and Environmental Engineering, University of Science and Technology Beijing

30 Xueyuan Road, Beijing 100083, China

* E-mail of the corresponding author: elias@xs.ustb.edu.cn

This research was supported by National International Cooperation Base on Environment and Energy, China.

Abstract

The low adsorption capacity and structural limitations of conventional geopolymers hinder their application in wastewater treatment. This study addresses these challenges by developing a carbonated fly ash-steel slag-based geopolymer (GP) for efficient Crystal Violet (CV) dye removal. Carbonated GP (GP-C) was synthesized via alkali activation and CO_2 curing, achieving a 91.66% removal efficiency and 6.11 mg/g adsorption capacity (vs. 76.04% and 5.07 mg/g for non- carbonated GP). BET analysis confirmed that carbonation increased the specific surface area from 13.14 m^2/g to 56.70 m^2/g by refining mesopores from 15–40 nm to 5–15 nm, enhancing adsorption efficiency. while FTIR/XPS identified key mechanisms: (1) hydrogen bonding between CV and hydroxyl groups (Si-OH) and (2) electrostatic attraction between CV^+ and aluminosilicate gels ($[AlO^4]^{4-}$/$[SiO^4]^{4-}$). The adsorption adhered to the Freundlich isotherm (heterogeneous surface) and pseudo-second-order kinetics. GP-C also exhibited broad pH adaptability (optimal at pH 9) and rapid equilibrium (90 min). This work highlights the dual role of carbonation in enhancing porosity and surface reactivity, offering a sustainable strategy to repurpose industrial waste (steel slag/fly ash) for dye pollution remediation.

Keywords: geopolymer; carbonation; adsorption; crystal violet; fly ash; steel slag; industrial solid waste

DOI: 10.7176/JEES/15-2-06

Publication date: April 30th 2025

1. Introduction

With the advancement of industrialization, a growing volume of dye wastes from industrial processes are being released into sewage systems during the dyeing of materials such as textiles, leather, plastics, and cosmetics, numerous refractory dyes were discharged into the water body (Li *et al.*, 2010; Lee, Jong Jib, 2014; Roy *et al.*, 2018; Lellis *et al.*, 2019). It was predicted that over 800,000 tons of synthetic dyes were manufactured annually, which would pose significant environmental challenges and impact aquatic ecosystems (Mahardiani *et al.*, 2021). A variety of methodologies, including electrochemical oxidation (Zhang *et al.*, 2010), chemical reduction (Trinh *et al.*, 2021), adsorption (Doondani, Gomase, *et al.*, 2022; Khapre *et al.*, 2022), and ion-exchange (Raghu and Ahmed Basha, 2007), have been employed to facilitate the removal of dyes. Among these methodologies, adsorption has emerged as a widely utilized and economically viable technique for the elimination of dyes from industrial effluents (Doondani, Jugade, *et al.*, 2022). Numerous substances, such as activated carbon, zeolites, and biochar, can serve as effective adsorbents within the adsorption process (Vithalkar and Jugade, 2020), which includes the accumulation of adsorbates at the liquid-solid or gas-solid interface (Kaykhaii, Sasani and Marghzari, 2018; Li *et al.*, 2020).

The alkali activation of waste materials has emerged as a significant area of research due to the potential for utilizing industrial byproducts such as ground granulated blast furnace slag (GGBFSS) and fly ash (FA) to transform them into environmentally friendly, cost-effective, and technologically beneficial cementitious materials, while also reducing carbon dioxide emissions (Nobouassia Bewa *et al.*, 2018; Salimi and Ghorbani, 2020). Davidovits (T. *et al.*, 2022) described geopolymer as an amorphous alumino-silicate cementitious material produced from natural aluminosilicates or industrial by-products, such as metakaolin, fly ash, and ground granulated blast furnace slag. The alkali activation of aluminosilicate raw materials appears through polymerization in a high pH environment. The polymerization reaction involves the development of three-

dimensional polymeric chains by Si-Al minerals, resulting in a ring structure that includes Si-O-Si bonds (Rajerajesw, Dhinakaran and Ershad, 2014). Such binders could handle the challenges faced by the construction industry. Geopolymer significantly reduces CO_2 emissions by 80%, offering a more economical solution while utilizing industrial and agricultural wastes (Singh, 2020; Singh and Middendorf, 2020). Numerous studies demonstrate that various industrial waste materials have been utilized as sources of alumina and silica for the preparation of geopolymers (Singh, Tripathy and Ranjith, 2008; Singh and Middendorf, 2020; Jindal *et al.*, 2022). Slag utilized as a base material consists of aluminosilicate raw material that can be triggered by alkali hydroxide and silicate (Singh, Tripathy and Ranjith, 2008). The alkali activation of slag results in an output product similar to calcium silicate hydrates (C-S-H) gel. Several studies have investigated the combined use of slag with industrial byproducts, including fly ash (FA), cement kiln dust (CKD), and silica fume (SF) (Phoo-ngernkham *et al.*, 2015; Kishar, Ahmed and Mahmoud, 2018; Kishar, Ahmed and Nabil, 2018; Elyamany, Abd Elmoaty and Diab, 2022). Geopolymers are suitable in various applications, including refractory and heat-resistant coatings, adhesives, pharmaceutical applications, novel adhesives for refractory fiber composites, wastewater treatment of toxic and radioactive waste, and innovative cement materials for concrete. In recent years, geopolymers have become popular as significant adsorbents due to their affordability, easy preparation, and individual three-dimensional network structure with fixed-size pores, that lets them adsorb the pollutants such as dyes and hazardous substances from the environment (Siyal *et al.*, 2018). Recent research has indicated the potential of geopolymer cements as adsorbents for the removal of different types of dyes (El Alouani *et al.*, 2019; Maleki *et al.*, 2020; Feng *et al.*, 2022), which demonstrated that the geopolymer showed significant adsorption capacity. Most of these current studies focus mainly on the gelation time, mechanical properties, and reaction mechanisms of rice husk (RH), rice husk ash (RHA), metakaolin (MK), palm oil fuel ash (POFA), ground granulated blast furnace slag (GGBFS), and slag systems, while there is little research on fly ash (FA) and steel slag (SS) based Geopolymers adsorption properties.

Several studies have highlighted the beneficial effects of carbonation on the microstructure and adsorption properties of cementitious materials. Carbonation enhances the specific surface area by refining pore structures and increasing the availability of adsorption sites (Liu *et al.*, 2022). It also improves nitrogen adsorption in cement-lime pastes, suggesting the formation of additional nanoscale pores that contribute to enhanced adsorption capacity (Arandigoyen *et al.*, 2006). Furthermore, carbonation plays a crucial role in optimizing the pore network, leading to a more interconnected and reactive surface. These improvements collectively make carbonated geopolymers highly effective for adsorption applications, offering both increased surface reactivity and structural stability (Silva *et al.*, 2002). Investigating the adsorption behaviour of carbonated Geopolymer and exploring the adsorption mechanism is a beneficial work.

This study focuses on developing carbonated geopolymer using industrial byproducts, fly ash and steel slag, as alternative adsorbents for the removal of the Crystal Violet (CV) dye residual in the dyeing bath instead of dumping this hazardous waste without treatment, as a new approach that is environmentally safe and inexpensive.

2. Materials and methods

2.1 Raw materials

The steel slag (SS) used in this study was sourced from a steel manufacturing plant in Jiangsu, China, while the fly ash (FA) was obtained from a power plant in Inner Mongolia, China. Prior to use, both materials were sieved through 100-mesh and 200-mesh screens to achieve the desired particle size distribution. The chemical compositions of SS and FA were analyzed using X-ray fluorescence (XRF), with the results summarized in Table 1.

Table 1. Chemical Composition of Steel Slag (SS) and Fly Ash (FA).

	SiO_2	Al_2O_3	CaO	Fe_2O_3	MgO	MnO	Other
SS	12.87	2.57	45.62	26.77	3.57	4.48	4.12
FA	45.51	45.86	1.58	2.40	0.27	0.02	4.36

As shown in Table 1, the major oxides present in SS included CaO, Fe_2O_3, and SiO_2, whereas FA was predominantly composed of SiO_2 and Al_2O_3. X-ray diffraction (XRD) analysis (Figure 3) revealed that the primary crystalline phases in SS were Larnite (Ca_2SiO_4), Lime (CaO), Srebrodolskite ($Ca_2Fe_2O_5$), Mayenite $(CaO)_{12}(Al_2O_3)_7$ and Wustite (FeO). In contrast, fly ash mainly consisted of mullite ($Al_{1.272}Si_{0.728}O_{4.864}$). For

alkali activation, granular sodium hydroxide (NaOH, AR grade, Sinopharm Chemical Reagent Co., Ltd., China) and industrial-grade sodium silicate (Na_2SiO_3, modulus = 2.05) were used. Additionally, 30% hydrogen peroxide (H_2O_2, AR grade, Sinopharm Chemical Reagent Co., Ltd., China) served as the foaming agent.

2.2 Preparation of Geopolymer (GP)

The Pictorial representation of synthesis process of Geopolymer (GP) for the application of GP in CV adsorption tests is shown in Figure 1. The procedure for preparing GP for CV adsorption was as follows: 120 g of steel slag and 30 g of fly ash were mixed at a low speed for 3 min using a mixer. Afterwards, 75 g of alkaline activator was measured, holding a liquid-to-solid mass ratio of 0.5. The liquid ingredient had been mixed with the solid mixtures for 1 min. Following that, 5 g of hydrogen peroxide was added and mixed at high speed for no more than 10 seconds. The mixed slurry was poured into molds and cured at 70℃ in an oven curing box for 24 hours. The samples were categorized into two categories upon successful demolding. One group was cured under standard indoor conditions and labeled as non-carbonated GP (GP-NC), and the other group was labeled as carbonated GP (GP-C) and cured in a CO_2 curing chamber for 24 hours.

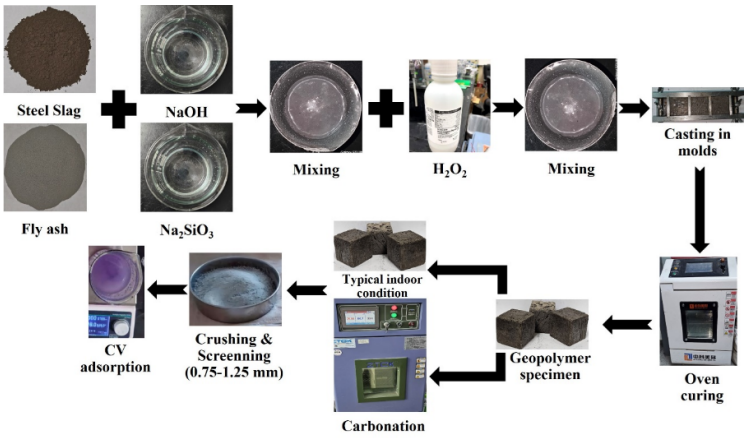

Figure 1. GP preparation and CV adsorption experiments pictorial representation.

The parameters in the CO_2 curing chamber have been set at a CO_2 concentration of 30%, a temperature of 30°C, and a humidity level of 90%. After 24 hours curing period, samples from both groups were crushed and sieved in order to get 0.75-1.25 mm particles for further adsorption experiments with CV.

2.3 Materials characterization

The following characterization techniques were employed to analyze the structural, chemical, and morphological properties of the raw materials and synthesized geopolymers:

2.3.1 Elemental Analysis

The crystalline phases present in raw steel slag, fly ash, and geopolymer samples were characterized using X-ray diffraction (XRD, Bruker D8 Advance, Germany) with Cu-Kα radiation (λ = 1.5406 Å). XRD patterns were collected over a 2θ range of 10-90° to identify mineralogical changes occurring during geopolymerization and carbonation processes. Complementary chemical bonding information was obtained through Fourier-transform infrared spectroscopy (FTIR, Thermo Scientific Nicolet iS20, USA). Spectra were acquired in the 400-4000 cm^{-1} range with 4 cm^{-1} resolution, allowing identification of functional groups and monitoring of structural transformations. The bulk chemical composition of raw materials was quantitatively determined by X-ray fluorescence spectroscopy (XRF, Analytical Axios, Netherlands). This technique provided precise oxide composition data essential for understanding material reactivity.

2.3.2 Morphological Analysis

Sample morphology and surface features were investigated using field-emission scanning electron microscopy (FE-SEM, Tescan MIRA3, Czech Republic). Multiple sample regions were examined to ensure representative imaging of microstructural evolution after carbonation treatment. Textural properties including specific surface area, pore size distribution, and total pore volume were measured through nitrogen physisorption using a Micromeritics TriStar II 3020 analyzer (USA). The Brunauer-Emmett-Teller (BET) method was applied to surface area calculations, while pore size distributions were derived from the adsorption branches using the Barrett-Joyner-Halenda (BJH) model.

2.4 Crystal violet adsorption studies

The adsorption efficacy of the produced Geopolymer (GP) adsorbent had been assessed using a Crystal Violet (CV) dye solution ($C_{25}H_{30}N_3Cl$; Cas No: 548-62-9; molecular weight 407.98) from Shenyang Chemical Reagent Factory, China; chemical structure of Crystal Violet (Figure 2.).

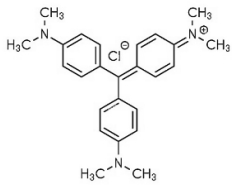

Figure 2. Chemical structure of Crystal Violet (CV).

A stock solution of CV with a concentration of 500 mg/L was made for further investigations. Adsorption reactions were conducted at 650 rpm using a magnetic stirrer under various conditions, with 200 mL of a defined concentration of CV solution and specified quantities of the adsorbent added into a series of 500 mL beakers. The solution matrix was centrifuged at 10,000 r/min for 5 minutes to extract the supernatant after each experiment met its adsorption conditions. Subsequently, a UV-Vis spectrophotometer (Shimadzu, UV-2700i, λmax = 590 nm) was used to figure out the CV concentration left in the supernatant.

A calibration curve was developed using a standard CV solution with some known concentrations. The adsorption tests were conducted three times to ensure accuracy, and the average value were taken into account. The removal efficiency (R%) and equilibrium adsorption capacity (Q_e, mg/g) of the two adsorbents for CV were calculated using Eq. 1 and Eq. 2, respectively.

$$R(\%) = \frac{C_o - C_e}{C_o} \times 100 \quad \text{(Eq. 1)}$$

$$Q_e(mg/g) = \frac{(C_o - C_e) \times V}{m} \quad \text{(Eq. 2)}$$

C_o and C_e represent the initial and equilibrium concentrations of CV (mg/L), respectively. V (L) denotes the volume of the solution at equilibrium, and m (g) is the mass of the adsorbent used. The anticipated pKa values of crystal violet are 5.31 and 8.64 (Rojas *et al.*, 2019), indicating that this molecule mostly exists in its cationic form in the environment.

2.4.1 The effect of adsorbent type

A mixture of the geopolymer sample (3 g) and a 100 mg/L CV solution was stirred at room temperature (26°C) and natural pH of the samples to study the effect of carbonation. Both types of geopolymer adsorbents, GP-NC and GP-C, were used. The experiments were conducted over a range of contact times from 0 to 120 minutes until the adsorption process reaches equilibrium. The removal efficiency and adsorption capacity were measured after each interval to evaluate the adsorption behaviour of the geopolymer samples over time.

2.4.2 The effect of contact time

To examine how contact time affected the geopolymer sample's ability to absorb dye, 100 mg/L of CV solution and 3 g of the geopolymer sample were mixed at room temperature (26°C), and natural pH of the adsorbent. The removal efficiency and adsorption capacity were calculated at contact times ranging from 5 minutes to 120 minutes.

2.4.3 The effect of dye concentration

The effect of initial dye concentration on the adsorption performance was investigated by varying the CV concentration from 10 mg/L to 100 mg/L, while maintaining a fixed geopolymer dosage of 3 g. The experiments were conducted at the natural pH of each geopolymer sample and stirred for 120 minutes at room temperature (26 °C). After equilibrium was reached, the final dye concentration was measured, and the removal efficiency along with the adsorption capacity was calculated.

2.4.4 The effect of adsorbent dosage

The equilibrium concentration was measured at various geopolymer dosages, and the removal efficiency and adsorption capacity were calculated. The experimental conditions were 100 mg/L CV solution at natural pH of the geopolymer and room temperature (26°C).

2.4.5 The effect of pH value

A mixture of the geopolymer sample and a 100 mg/L CV solution was stirred at room temperature (26°C) at

various pH values ranging from 2.0 to 11.0. Dilute hydrochloric acid (HCl), 1 mol/L and sodium hydroxide (NaOH), 1 mol/L were used to adjust the pH. The removal efficiency and adsorption capacity were measured when the system reached equilibrium.

3. Results and discussion

3.1 Characterization of GP

3.1.1 Elemental analysis

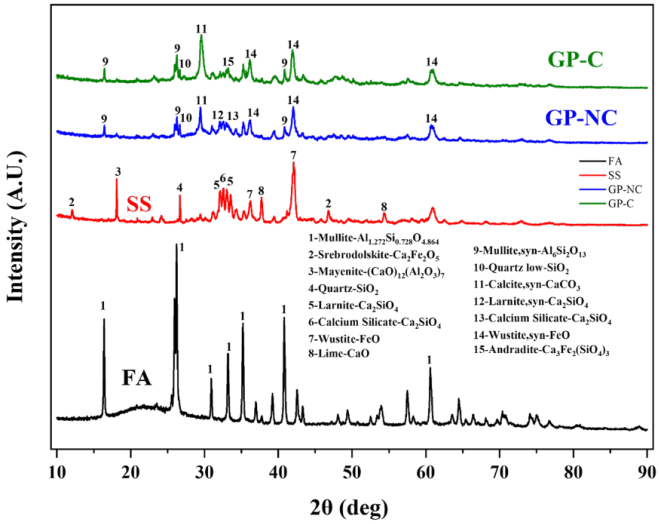

Figure 3. XRD study illustrating the mineral phases present in SS, FA, GP-NC and GP-C samples.

The XRD patterns showed that the crystalline phase composition of GP-NC and GP-C primarily comprised quartz (SiO_2), calcium iron garnet (andradite, $Ca_3Fe_2(SiO_4)_3$), calcium silicate (Ca_2SiO_4), and calcite ($CaCO_3$), shown in Figure 3. A broad peak observed in the 25°-45° 2θ range suggests the presence of amorphous or semi-crystalline materials, likely corresponding to the main reaction products, sodium aluminate hydrate (N-A-S-H) gel and calcium aluminate hydrate (C-A-S-H) gel. (Liu *et al.*, 2019, 2024), (He *et al.*, 2022). The formation of C(N)-A-S-H gel was a notable indication of geopolymerization. Furthermore, upon carbonation, the diffraction peaks of GP-C in the 30°-50° range exhibited increased sharpness and intensity, further confirming the enhanced production of $CaCO_3$ as a result the carbonation reaction (Li *et al.*, 2022).

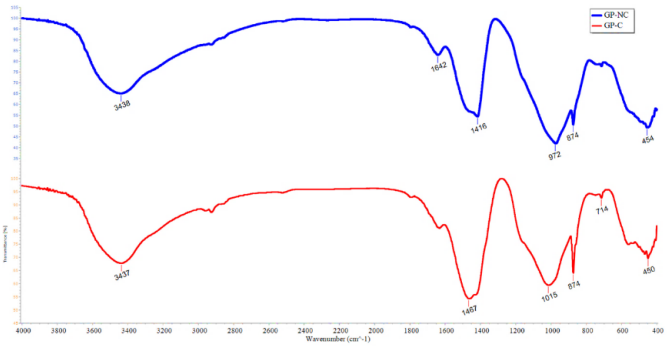

Figure 4. FTIR spectra of geopolymer samples GP-NC and GP-C.

The FTIR spectra of GP-NC and GP-C reveal distinct changes after carbonation, particularly in the appearance of new absorption bands (Menges, no date), in Figure 4. Both samples show a broad band around 3438 cm^{-1}, corresponding to hydroxyl (-OH) stretching vibrations, indicating the presence of water or surface hydroxyl groups. The Si-O-Si asymmetric stretching vibration at 972 cm^{-1} in GP-NC reflects the aluminosilicate network typical of geopolymers. After carbonation, GP-C exhibits new peaks: the band at 714 cm^{-1} is attributed to the C=O bond vibration in calcite, while the band at 874 cm^{-1} corresponds to the out-of-plane bending of the C=O

bond in calcite. Additionally, the broad peak at 1467 cm^{-1} is linked to the CO_3^{2-} stretching vibration, further confirming the formation of carbonate groups (Chang *et al.*, 2019; Zhang *et al.*, 2024). These changes suggest that carbonation has led to the formation of calcite and other carbonates, significantly altering the material's structure and surface properties. The absorption bands confirmed the existence of carbonation reaction and the creation of carbonation products (Matalkah and Soroushian, 2023). In addition, the absorption bands at 1642 cm^{-1} and 3437 cm^{-1} correspond to the bending and stretching vibrations of O-H in water molecules, respectively (Wei *et al.*, 2020; H. Liu *et al.*, 2021; Kravchenko *et al.*, 2023). The O-H stretching vibration at 3437 cm^{-1} exhibits a similar profile to that of GP-NC, suggesting that activation enhances the population of hydroxyl (Ma *et al.*, 2024).Fly ash addition promoted C-S-H gel decalcification in a CO_2-rich environment, resulting in a lower Ca/Si ratio and increased silicate polymerization (Chen *et al.*, 2024).

Table 2. Average contact angle of GP-NC and GP-C.

Material	Contact angle/°	Average contact angle/°
GP-NC	15.372	15.526
	15.525	
	15.680	
GP-C	15.222	15.141
	15.076	
	15.124	

Moreover, this increase in oxygen-containing functional groups contributed to a slight improvement in surface hydrophilicity, as evidenced by water contact angle measurements. The average contact angle decreased from 15.526° for GP-NC to 15.141° for GP-C after carbonation treatment (Table 2), further confirming the improved hydrophilic nature of the material surface as a result of carbonation.

3.1.2 Morphological analysis

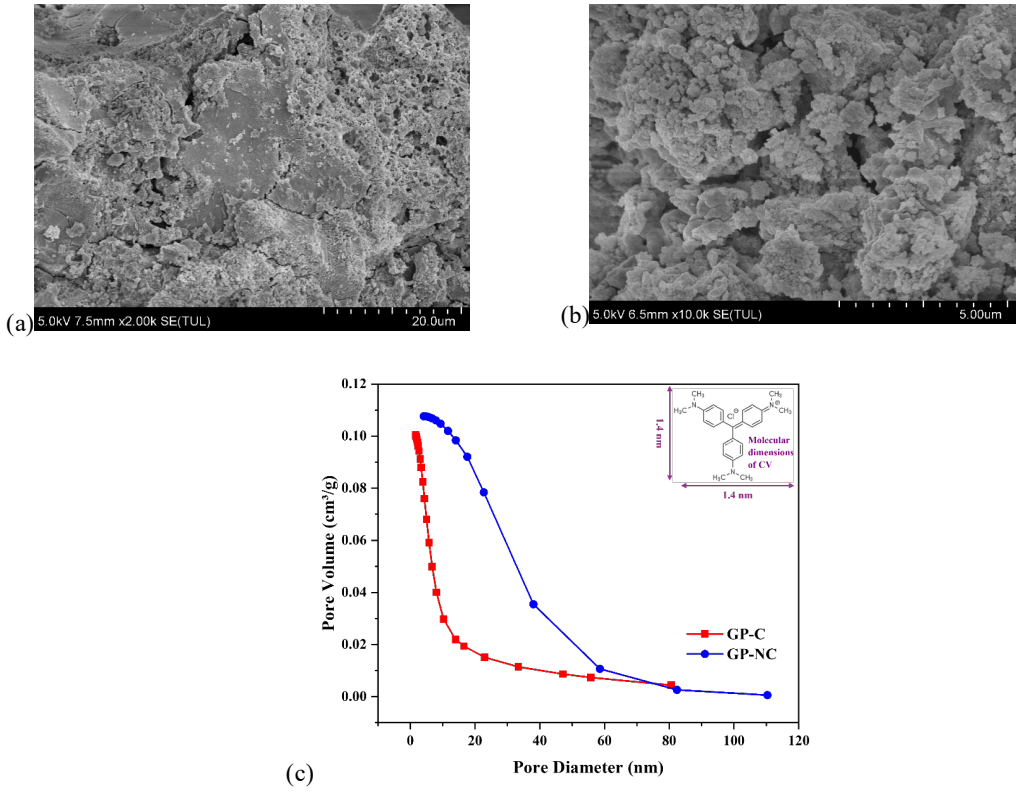

Figure 5. SEM micrographs showing the surface morphology of (a) GP-NC, (b) GP-C samples; (c) The pore size distribution of the GP-NC and GP-C samples.

The SEM analysis of GP-NC and GP-C clearly highlights the structural differences between the two samples, in line with the observed changes in their specific surface area. As shown in Figure 5a, the surface of GP-NC is relatively smooth with limited pore development, suggesting fewer surface features and a more uniform structure. In contrast, Figure 5b reveals that after carbonation, the surface of GP-C exhibits a significant transformation. The presence of microcrystalline calcium carbonate, including cubic calcite and rod-shaped aragonite, indicates the formation of carbonation products that adhere to the surface. These products contribute to an increase in surface roughness and a greater number of smaller pores, which is consistent with the enhanced specific surface area of GP-C. During carbonization, reaction products gradually built up along the inner walls of the pores, a trend clearly visible in the pore size distribution data (Figure 5c). This created two important changes in the material's structure: First, it partially filled some of the larger mesopores, forming a network of tiny micropores. Second, it made the surface more textured and uneven. Interestingly, these structural shifts turned out to be ideal for trapping crystal violet (CV) molecules. As the inset shows, CV measures about 1.4 nm in size, which is small enough to fit into the newly formed micropores. The material now had a mix of larger macropores (which help molecules move freely) and smaller micropores (which maximize surface area for adsorption). Together, these features boosted the material's ability to capture and hold CV molecules efficiently. The specific surface area of GP-NC was measured at 13.1386 m^2/g, while that of GP-C reached 56.6997 m^2/g, as shown in Table 3. Carbonation treatment increased the specific surface area of GP-C by more than four times relative to GP-NC. Our previous study suggested that this substantial increase in surface area contributed to a higher number of active adsorption sites, thereby enhancing the overall adsorption capacity through improved interactions between the active sites and the adsorbate.

Table 3. Pore structure characteristic.

Material	BET surface area m^2/g	Average pore diameter nm	Total pore volume cm^3/g
GP-NC	13.1386	30.84984	0.101331
GP-C	56.6997	7.09036	0.100505

Crystal violet (CV), a cationic triphenylmethane dye with molecular dimensions of approximately 1.4 nm × 1.4 nm (Wathukarage *et al.*, 2019; Azhar-ul-Haq *et al.*, 2024), demonstrates enhanced adsorption in engineered mesoporous systems. As shown in Figure 5c, while both GP-NC and GP-C exhibit mesoporous structures (2-50 nm), carbonation significantly modified the pore architecture; GP-NC's broad pore distribution (15-40 nm, average 30 nm) transitioned to GP-C's narrower range (5-15 nm, average 7 nm) through selective infilling of larger pores by carbonation products. This structural refinement yielded three key advantages for CV adsorption: (1) the 7 nm pores provide optimal size matching to the 1.4 nm CV molecules, enabling effective molecular confinement; (2) the 4.3 times increase in surface area (56.7 vs 13.1 m^2/g) creates more accessible binding sites; and (3) the preserved pore volume (0.1005 cm^3/g) maintains efficient mass transport despite pore size reduction. These synergistic effects explain GP-C's superior CV adsorption capacity compared to GP-NC.

3.2 CV adsorption studies

3.2.1 Types of Adsorbents

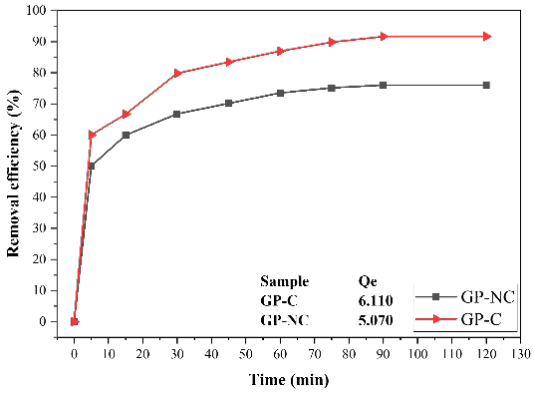

Figure 6. Removal efficiency of CV by GP-NC and GP-C.

The adsorption effects of GP-NC and GP-C on CV were analyzed under identical conditions using 3 g of adsorbent, room temperature (26°C) and 100 mg/L of CV solution at its natural pH. In both cases, GP-NC and GP-C followed three distinct stages over time: a rapid stage, a medium-speed stage, and a slow stage. The results indicated that both adsorbents demonstrated significant affinity for CV, with GP-C showing a higher adsorption capacity compared to GP-NC. Figure 6 showed that the optimal removal efficiency and adsorption capacity of GP-C for CV were 91.66% and 6.11 mg/g, respectively. The values for GP-NC were lower, recorded at 76.04% and 5.07 mg/g. The results indicated that carbonation treatment enhances the adsorption capacity of GP for CV. The finding suggests that the structural properties of GP-C may enhance its effectiveness in capturing CV molecules from the solution. Therefore, we have selected GP-C for the upcoming experiments.

3.2.2 Effect of contact time

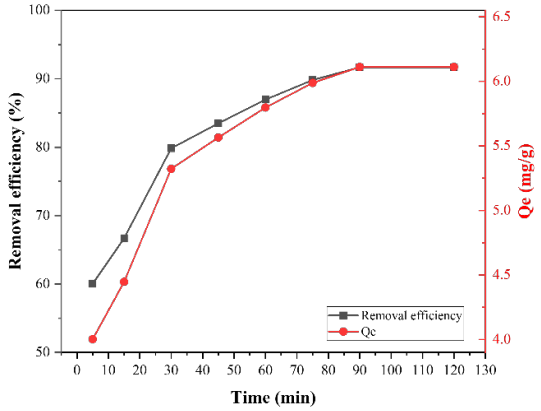

Figure 7. Effect of Contact time on CV by GP-C.

The effects of contact time on CV adsorption by GP-C at room temperature (26 °C) revealed a three-stage adsorption process: a rapid stage, a medium-speed stage, and a slow stage. Other parameters were kept constant, including 3 g of adsorbent, 100 mg/L of CV solution, and the natural pH of the adsorbent. As Shown in Figure 7, in the initial rapid stage, most of the dye was removed within the first 30 minutes due to the high availability of active adsorption sites on the adsorbent surface. As time progressed into the medium-speed stage, the removal rate gradually decreased as the available sites became occupied. Finally, in the slow stage, after 60 minutes, the adsorption process reached equilibrium, with minimal changes in removal efficiency. At this point, the active sites were nearly saturated with CV molecules, and further adsorption was limited, as attachment and detachment occurred at the same rate after 90 minutes. Extending the contact time beyond this stage did not significantly improve dye removal. The time required for the dye adsorption process to reach equilibrium was determined to be 90 minutes, and therefore, this time was selected as the optimal contact time. The optimal removal efficiency and adsorption capacity of GP-C for CV were 91.66% and 6.11 mg/g, respectively.

3.2.3 Effect of initial dye concentration

The effects of the initial dye concentration on the removal efficiency were investigated by varying the dye concentrations, while keeping other parameters constant: 3 g of adsorbent, room temperature (26 °C), and the natural pH of the solution. As shown in Figure 8, The adsorption capacity and removal efficiency increased with increasing dye concentration (Mužek, Svilović and Zelić, 2014; Sun *et al.*, 2023). When the initial CV concentration increased from 10 mg/L to 100 mg/L, the amount of dye adsorbed also increased. The removal efficiencies were 83.0%, 85.31%, 88.61%, 91.66% for the 10mg/L, 20 mg/L, 50 mg/L and 100mg/L CV solutions, respectively. Similarly, the adsorption capacity increased from 5.53 mg/g for the 10 mg/L solution to 6.11 mg/g for the 100 mg/L solution.

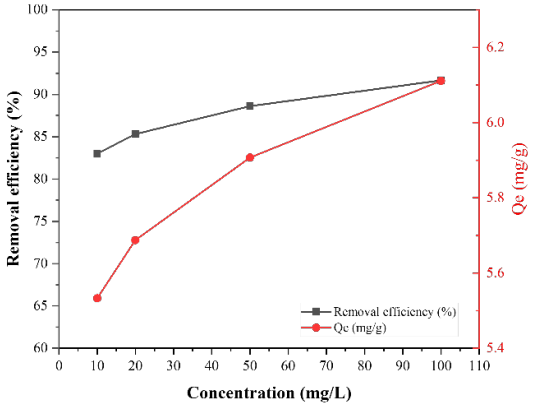

Figure 8. Effect of initial dye concentration on CV by GP-C.

This trend indicates that at lower dye concentrations, a sufficient number of available pores in the geopolymer facilitated higher adsorption. The adsorption capacity and removal efficiency of GP-C for CV increased with higher initial concentrations of CV.

3.2.4 Effect of adsorbent dosage

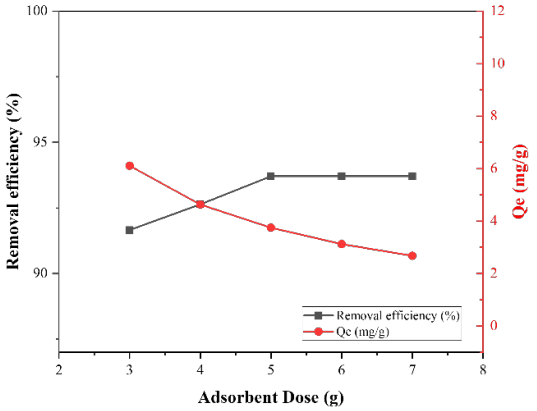

Figure 9. Effect of adsorbent dosage on CV by GP-C.

As the dosage of GP-C increased from 3 to 5 grams, the removal efficiency of Crystal Violet (CV) dye improved from 91.67% to 93.71%, while keeping all other parameters constant (CV concentration: 100 mg/L, room temperature: 26 °C, and natural pH of the solution); however, further increasing the dosage to 7 grams resulted in negligible improvement. Indeed, the dye adsorption from solution on the adsorbent material increased as the amount of the geopolymer increased (Xu, 2008; Al-Zboon, Al-Harahsheh and Hani, 2011). As shown in Figure 9, the removal efficiency increased initially and then stabilized, while the adsorption capacity decreased significantly. The enhanced removal efficiency can be attributed to the greater number of active sorption sites on the geopolymer surface, but beyond a certain dosage, the adsorption process reached saturation, where additional adsorbent did not significantly improve dye removal. This highlights the need for an optimal adsorbent dosage to achieve maximum efficiency while maintaining stable adsorption capacity. Moreover, increasing the adsorbent dosage simultaneously reduced the number of dye molecules adsorbed per unit of adsorbent, leading to a decline in adsorption capacity. This is because the total number of CV molecules remains constant for a given volume and concentration of the CV solution, and adding more adsorbent decreases the driving force for each active site, thereby reducing adsorption capacity.

3.2.5 Effect of pH

The pH of the solution significantly influences the adsorption process by affecting the surface charge of the adsorbent, the ionization of the adsorbate, and the speciation of adsorbate species, which play a critical role in dye removal (Mushtaq *et al.*, 2016). In this study, the effect of pH on CV adsorption was evaluated over a pH

range of 3 to 11 using 3 g of GP-C, a contact time of 90 minutes, and an initial dye concentration of 100 mg/L at room temperature (26 °C). The CV removal efficiency increased with rising pH and reached a maximum at pH 9. However, beyond this point, a further increase in pH led to a gradual decline in adsorption capacity (Figure 10a). This trend may be attributed to the change in the protonation state of functional groups on the geopolymer surface, which can be protonated in acidic media and deprotonated under basic conditions. These changes influence the surface charge, affecting electrostatic interactions with the cationic dye molecules (CV). At mildly basic pH, the surface likely becomes negatively charged, favoring electrostatic attraction toward CV. Conversely, under highly basic conditions (pH > 9), the formation of excess hydroxyl ions may compete with dye molecules for adsorption sites, leading to decreased removal efficiency (Ajmal *et al.*, 2000; Yao, Qi and Wang, 2010). Under acidic conditions, a high concentration of H_3O^+ ions compete with dye molecules for active binding sites, and the electrostatic repulsion between the positively charged surface and the cationic CV molecules may hinder adsorption. Similar pH-dependent behavior has been reported for other bioadsorbents, such as bark (Ahmad, 2009) and apple shell waste (Jain and Jayaram, 2010), where low adsorption at acidic pH was correlated with surface protonation and reduced electrostatic attraction.

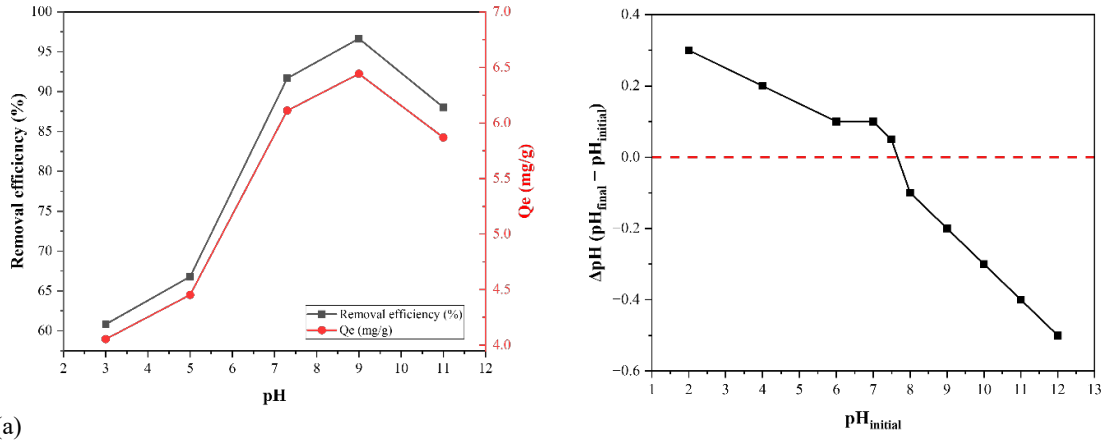

(a) (b)

Figure 10. (a) Removal efficiency of CV by GP-C, Effect of pH; (b) pH_{pzc} of GP-C.

According to the literature (Sarma and Mahiuddin, 2014), the point of zero charge (pH_{pzc}) of the GP-C adsorbent was determined to be 7.49 (Figure 10b). This value indicates that the adsorbent surface is positively charged at pH < 7.49 and negatively charged at pH > 7.49. Considering the pKa values of crystal violet (5.31 and 8.64) (Rojas *et al.*, 2019), the optimal pH for adsorption lies in a region where the GP-C surface is negatively charged and CV remains in its cationic form, facilitating electrostatic attraction and enhancing dye removal.

3.3 Isotherm model studies and kinetic studies

3.3.1 Langmuir and Freundlich isotherm models

An isothermal adsorption study was conducted at room temperature over a duration of 120 minutes to ensure adsorption equilibrium. The initial concentrations of CV ranged from 10 to 100 mg/L. To investigate the equilibrium adsorption behavior of CV onto the geopolymer samples, both the Langmuir and Freundlich isotherm models were employed. The mathematical expressions corresponding to these models are presented as Eq. 3 and Eq. 4, respectively:

$$\text{Langmuir: } \frac{C_e}{Q_e} = \frac{1}{Q_{max} K_L C_e} + \frac{C_e}{Q_{max}} \quad \text{(Eq. 3)}$$

$$\text{Freundlich: } \ln Q_e = \ln K_F + \frac{1}{n} \ln C_e \quad \text{(Eq. 4)}$$

In these equations, C_e (mg/L) represents the equilibrium concentration of CV in solution, Q_{max} (mg/g) is the maximum monolayer adsorption capacity, and K_L (L/mg) denotes the Langmuir constant related to the affinity of binding sites. For the Freundlich model, K_F (L/mg) is the Freundlich constant indicating adsorption capacity, and n is a dimensionless parameter that reflects adsorption intensity and surface heterogeneity.

Table 4. Isotherms parameters of CV adsorption on GP-C.

Langmuir			Freundlich		
Q_{max} (mg/g)	b (L/mg)	R^2	k_F (L/mg)	1/n (mg/L)	R^2
3.98	-0.074	0.9882	0.0847	0.6646	0.9975

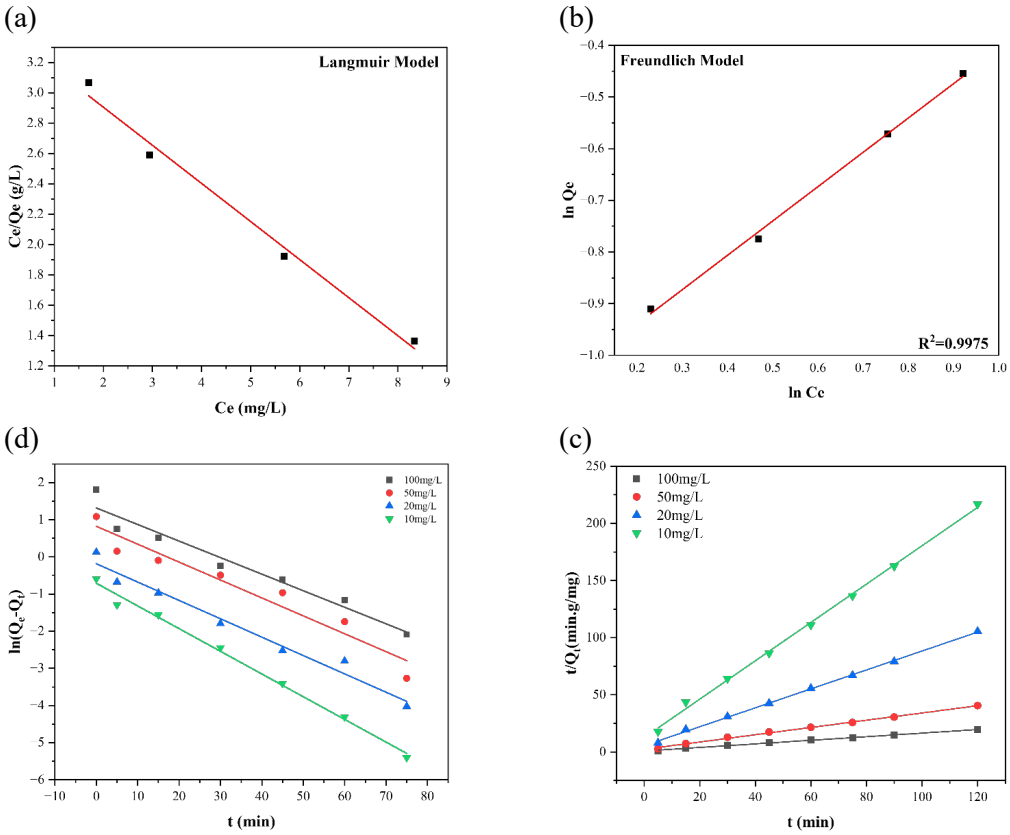

Figure 11. Linear fitting of - a) Langmuir isotherm; b) Freundlich isotherm; c) pseudo-first-order kinetic model; d) pseudo-second-order kinetic model.

Results were shown in Table 4, Figure 11a and 11b, respectively. The comparison of R^2 values for the Langmuir and Freundlich isotherm models indicated that the adsorption of CV onto the GP-C fits better with the Freundlich model, which had a higher R^2 value of 0.9975. The Freundlich isotherm describes adsorption on heterogeneous surfaces and is widely used to represent multilayer adsorption behavior (Wang and Guo, 2020). The CV molecules were likely adsorbed onto the GP-C surface via multiple active sites with varying affinities. The 1/n value of 0.6646 (where $0 < 1/n < 1$) implies favorable adsorption and a strong interaction between the CV molecules and the GP-C surface. These results demonstrate that GP-C provides suitable surface characteristics and porosity for CV adsorption, where increasing the number of adsorption sites could potentially enhance the overall adsorption performance (Zhou, Ma and Guo, 2020).

3.3.2 Pseudo-first-order and Pseudo-second-order

The adsorption kinetics were analyzed using pseudo-first-order and pseudo-second-order models (Eq. 5 and Eq. 6, respectively), with the corresponding fitting results illustrated in Figure 11c and 11d and summarized in Table 5.

$$Ln(Q_e - Q_t) = LnQ_e - K_1 t \quad \text{(Eq. 5)}$$

$$\frac{t}{Q_t} = \frac{1}{K_2 Q_e^2} + \frac{t}{Q_e} \quad \text{(Eq. 6)}$$

In these models, Q_t (mg/g) represents the amount of CV adsorbed at time t (min). The rate constants are denoted as K_1 (1/min) and K_2 (g/(mg·min)), respectively.

Table 5. Kinetic parameters of CV adsorption on GP-C.

C_0 (mg/L)	Pseudo-first order kinetic model			Pseudo-second order kinetic model		
	Q_e (mg/g)	k_1 (g/(mg·min))	R^2	Q_e (mg/g)	K_2 (g/(mg·min))	R_2
10	0.492	0.0610	0.9931	0.596	0.2233	0.9978
20	0.831	0.0493	0.9730	1.207	0.1239	0.9988
50	2.278	0.0482	0.9349	3.146	0.0425	0.9968
100	3.729	0.0445	0.9522	6.388	0.0292	0.9989

C_0 (mg/L)	$Q_{experiment}$ (mg/g)	Pseudo-first order kinetic model			Pseudo-second order kinetic model		
		Q_e (mg/g)	k_1 (g/(mg·min))	R^2	Q_e (mg/g)	K_2 (g/(mg·min))	R^2
10	0.5535	0.5421	0.0251	0.9812	0.5550	0.1023	0.9999
20	1.1371	1.1125	0.0228	0.9785	1.1400	0.0456	0.9999
50	2.9546	2.9012	0.0203	0.9723	2.9600	0.0187	0.9999
100	6.1110	5.9800	0.0185	0.9610	6.1200	0.0089	0.9999

The pseudo-second-order model provided a better fit for CV adsorption on GP-C across all concentrations, as evidenced by higher R^2 values (0.9978-0.9989) compared to the pseudo-first-order model (0.9522-0.9931). The calculated Q_e values from the pseudo-second-order model (0.596-6.388 mg/g) closely matched the experimental data (0.5535-6.1110 mg/g), while the pseudo-first-order model underestimated the adsorption capacity. The maximum adsorption rate reached 0.2233 g/(mg·min) at the lowest CV concentration (10 mg/L), decreasing with increasing concentration due to site saturation. This kinetic behavior indicates the adsorption process is controlled by surface chemical reactions rather than simple diffusion.

4. Adsorption Mechanism for CV

The process of CV adsorption onto GP-C involves several key mechanisms working together. In water, CV breaks down into positively charged CV^+ ions and negatively charged Cl^- ions. Analysis through FTIR confirms that GP-C contains hydroxyl (OH) groups, which interact with the CV^+ ions (Batool *et al.*, 2021). When the adsorption process occurs in solution, the $[AlO^4]^{4-}$ and $[SiO^4]^{4-}$ in the C(N)-A-S-H gel structure of GP interact with CV^+ through electrostatic interactions, as CV is a typical cationic dye. Experimental data shows that as the pH increases, the amount of CV adsorbed onto GP-C also rises, suggesting that pH plays a key role in the adsorption process. The primary mechanism driving this adsorption is electrostatic attraction. The GP-C surface becomes negatively charged, which attracts the positively charged CV^+ ions, leading to the formation of an adsorbed complex. This can be described by the reaction between GP-C and hydroxide ions (OH^-), where the hydroxyl groups on the GP-C surface become negatively charged:

$$GP\text{-}C(Si\text{-}OH) + OH^- \rightarrow GP\text{-}C(Si\text{-}O^-) + H_2O$$

These negatively charged sites then attract the positively charged CV^+ ions:

$$GP\text{-}C(Si\text{-}O^-) + CV^+Cl^- \rightarrow GP\text{-}C(Si\text{-}O^-CV^+) + Cl^-$$

But electrostatic interactions aren't the only mechanism at play. Hydrogen bonding also contributes to the process. The Si-OH groups on GP-C form bonds with the nitrogen (N) atoms in CV molecules (Zhang *et al.*, 2022), further stabilizing the adsorbed dye:

$$GP\text{-}C(Si\text{-}OH) + CV \rightarrow GP\text{-}C(Si\text{-}OH\cdots N\text{-}CV)$$

Additionally, due to CV's triphenylmethane structure, π-π interactions occur between the aromatic rings of CV and the carbonated regions of GP-C (Nuñez *et al.*, 2019; J. Liu *et al.*, 2021). These interactions further strengthen the adsorption, helping to keep the CV molecules firmly attached to the surface. During the

carbonation of GP-C, CO_2 reacts with calcium ions, forming carbonate deposits that increase the surface area and provide more active sites for adsorption. Moreover, the decalcification process within the material's structure leads to a negative charge imbalance (Jin *et al.*, 2020). This is balanced by the oxygen in silicate chains, which captures positively charged species like silicon and hydrogen from water. This enhances the formation of Si-O-Si bonds, increasing the material's polymerization and improving its ability to interact with water, making it even more effective at adsorbing CV.

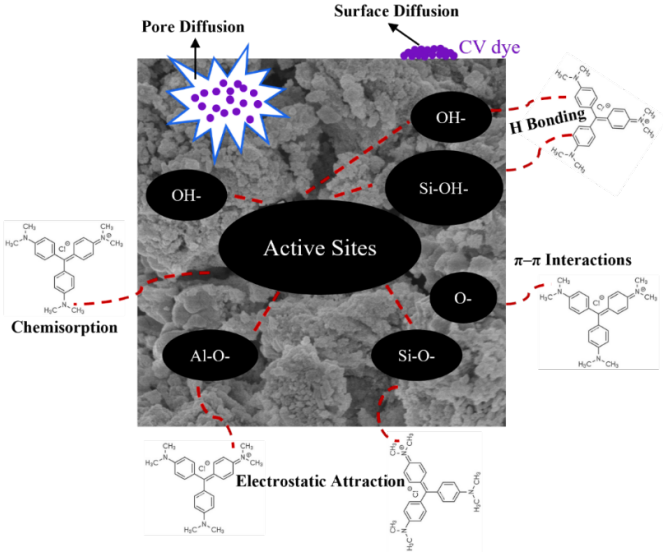

Figure 12. Proposed adsorption mechanism (CV and GP-C).

Overall, the combination of electrostatic attraction, hydrogen bonding, and π–π interactions makes GP-C an efficient material for removing CV from water. These mechanisms (Figure 12.) work together to ensure the dye is effectively adsorbed, demonstrating the material's potential as a powerful adsorbent.

5. Conclusion

This study successfully demonstrated that carbonation significantly improves the adsorption performance of fly ash-steel slag geopolymers for CV. Under optimized conditions (3 g adsorbent, 100 mg/L CV, pH 9), GP-C achieved a 91.66% removal efficiency and 6.11 mg/g adsorption capacity, surpassing GP-NC (76.04%, 5.07 mg/g). Key findings include:

1. Pore structure refinement: Carbonation reduced average pore size from 30 nm to 7 nm, increasing the BET surface area 4.3 times (from 13.13 to 56.70 m^2/g), and exposing more active sites.

2. Adsorption mechanisms: Synergistic effects of (i) electrostatic interactions between CV^+ and negatively charged $[AlO^4]^{4-}/[SiO^4]^{4-}$ gels and (ii) hydrogen bonding with surface Si-OH groups (confirmed by FTIR).

3. Kinetics and isotherms: The process followed the Freundlich model (multilayer adsorption) and pseudo-second-order kinetics ($R^2 > 0.997$), indicating chemisorption dominance.

4. pH resilience: GP-C performed optimally at pH 9 (near CV pKa = 8.64), with the pH_{pzc} (7.49) ensuring surface negativity for cationic CV attraction.

The study underscores the potential of carbonation technology to transform industrial byproducts (steel slag, fly ash) into high-efficiency, eco-friendly adsorbents. Future work could explore regeneration cycles and pilot-scale applications to advance practical implementation.

References

Ahmad, R. (2009) 'Studies on adsorption of crystal violet dye from aqueous solution onto coniferous pinus bark powder (CPBP)', *Journal of Hazardous Materials*, 171(1–3), pp. 767–773. Available at: https://doi.org/10.1016/j.jhazmat.2009.06.060.

Ajmal, M. *et al.* (2000) 'Adsorption studies on Citrus reticulata (fruit peel of orange): removal and recovery of

Ni(II) from electroplating wastewater', *Journal of Hazardous Materials*, 79(1–2), pp. 117–131. Available at: https://doi.org/10.1016/S0304-3894(00)00234-X.

Al-Zboon, K., Al-Harahsheh, M.S. and Hani, F.B. (2011) 'Fly ash-based geopolymer for Pb removal from aqueous solution', *Journal of Hazardous Materials*, 188(1–3), pp. 414–421. Available at: https://doi.org/10.1016/j.jhazmat.2011.01.133.

Arandigoyen, M. *et al.* (2006) 'Variation of microstructure with carbonation in lime and blended pastes', *Applied Surface Science*, 252(20), pp. 7562–7571. Available at: https://doi.org/10.1016/j.apsusc.2005.09.007.

Azhar-ul-Haq, M. *et al.* (2024) 'Adsorptive removal of hazardous crystal violet dye onto banana peel powder: equilibrium, kinetic and thermodynamic studies', *Journal of Dispersion Science and Technology*, 45(3), pp. 475–490. Available at: https://doi.org/10.1080/01932691.2022.2158851.

Batool, M. *et al.* (2021) 'Exploring the usability of Cedrus deodara sawdust for decontamination of wastewater containing crystal violet dye', *Desalination and Water Treatment*, 224, pp. 433–448. Available at: https://doi.org/10.5004/dwt.2021.27192.

Chang, J. *et al.* (2019) 'Foaming characteristics and microstructure of aerated steel slag block prepared by accelerated carbonation', *Construction and Building Materials*, 209, pp. 222–233. Available at: https://doi.org/10.1016/j.conbuildmat.2019.03.077.

Chen, Z. *et al.* (2024) 'Study on evolution of pores channel in carbonation steel slag samples with fly ash', *Construction and Building Materials*, 411, p. 134471. Available at: https://doi.org/10.1016/j.conbuildmat.2023.134471.

Doondani, P., Gomase, V., *et al.* (2022) 'Chitosan coated cotton-straw-biochar as an admirable adsorbent for reactive red dye', *Results in Engineering*, 15, p. 100515. Available at: https://doi.org/10.1016/j.rineng.2022.100515.

Doondani, P., Jugade, R., *et al.* (2022) 'Chitosan/Graphite/Polyvinyl Alcohol Magnetic Hydrogel Microspheres for Decontamination of Reactive Orange 16 Dye', *Water*, 14(21), p. 3411. Available at: https://doi.org/10.3390/w14213411.

El Alouani, M. *et al.* (2019) 'Preparation, Characterization, and Application of Metakaolin-Based Geopolymer for Removal of Methylene Blue from Aqueous Solution', *Journal of Chemistry*, 2019, pp. 1–14. Available at: https://doi.org/10.1155/2019/4212901.

Elyamany, H.E., Abd Elmoaty, A.E.M. and Diab, A.R.A. (2022) 'Properties of slag geopolymer concrete modified with fly ash and silica fume', *Canadian Journal of Civil Engineering*, 49(2), pp. 183–191. Available at: https://doi.org/10.1139/cjce-2019-0757.

Feng, X. *et al.* (2022) 'Green Synthesis of the Metakaolin/slag Based Geopolymer for the Effective Removal of Methylene Blue and Pb (II)', *Silicon*, 14(12), pp. 6965–6979. Available at: https://doi.org/10.1007/s12633-021-01439-z.

He, H. *et al.* (2022) 'Alkali-excited gel structure and compositions evolution in geopolymers synthesized from the spent FCC catalyst and steel slag', *Journal of Materials Research and Technology*, 21, pp. 2663–2671. Available at: https://doi.org/10.1016/j.jmrt.2022.10.057.

Jain, S. and Jayaram, R.V. (2010) 'Removal of basic dyes from aqueous solution by low-cost adsorbent: Wood apple shell (Feronia acidissima)', *Desalination*, 250(3), pp. 921–927. Available at: https://doi.org/10.1016/j.desal.2009.04.005.

Jin, S. *et al.* (2020) 'Effect of Corrosive Ions (Cl−, SO42−, and Mg2+) on the Nanostructure and Chloride Binding Property of C-A-S-H Gel', *Journal of Wuhan University of Technology-Mater. Sci. Ed.*, 35(6), pp. 1061–1072. Available at: https://doi.org/10.1007/s11595-020-2356-8.

Jindal, B.B. *et al.* (2022) 'Geopolymer concrete with metakaolin for sustainability: a comprehensive review on raw material's properties, synthesis, performance, and potential application', *Environmental Science and Pollution Research*, 30(10), pp. 25299–25324. Available at: https://doi.org/10.1007/s11356-021-17849-w.

Kaykhaii, M., Sasani, M. and Marghzari, S. (2018) 'Removal of Dyes from the Environment by Adsorption Process', *Chemical and Materials Engineering*, 6(2), pp. 31–35. Available at: https://doi.org/10.13189/cme.2018.060201.

Khapre, M. *et al.* (2022) 'Mesoporous Fe–Al-doped cellulose for the efficient removal of reactive dyes', *Materials Advances*, 3(7), pp. 3278–3285. Available at: https://doi.org/10.1039/D2MA00146B.

Kishar, E., Ahmed, D. and Mahmoud, A. (2018) 'Resistance of alkali-activated slag to sulphate attack and elevated temperatures', *Journal of Scientific Research in Science*, 35(part 1), pp. 63–77. Available at: https://doi.org/10.21608/jsrs.2018.11712.

Kishar, E., Ahmed, D. and Nabil, N. (2018) 'Geopolymer Cement Based on Alkali Activated Slag', *Journal of Scientific Research in Science*, 34(part1), pp. 538–552. Available at: https://doi.org/10.21608/jsrs.2018.14709.

Kravchenko, E. *et al.* (2023) 'Effect of polyvinyl alcohol on the CO2 uptake of carbonated steel slag', *Construction and Building Materials*, 375, p. 130761. Available at: https://doi.org/10.1016/j.conbuildmat.2023.130761.

Lee, Jong Jib (2014) 'Study on Equilibrium, Kinetic and Thermodynamic for Adsorption of Quinoline Yellow by Granular Activated Carbon', *Clean Technology*, 20(1), pp. 35–41. Available at: https://doi.org/10.7464/KSCT.2014.20.1.035.

Lellis, B. *et al.* (2019) 'Effects of textile dyes on health and the environment and bioremediation potential of living organisms', *Biotechnology Research and Innovation*, 3(2), pp. 275–290. Available at: https://doi.org/10.1016/j.biori.2019.09.001.

Li, F. *et al.* (2022) 'Effect of mixed fibers on fly ash-based geopolymer resistance against carbonation', *Construction and Building Materials*, 322, p. 126394. Available at: https://doi.org/10.1016/j.conbuildmat.2022.126394.

Li, P. *et al.* (2010) 'Bioadsorption of methyl violet from aqueous solution onto Pu-erh tea powder', *Journal of Hazardous Materials*, 179(1–3), pp. 43–48. Available at: https://doi.org/10.1016/j.jhazmat.2010.02.054.

Li, X. *et al.* (2020) 'Adsorption materials for volatile organic compounds (VOCs) and the key factors for VOCs adsorption process: A review', *Separation and Purification Technology*, 235, p. 116213. Available at: https://doi.org/10.1016/j.seppur.2019.116213.

Liu, C. *et al.* (2024) 'Structural evolution of calcium sodium aluminosilicate hydrate (C-(N-)A-S-H) gels induced by water exposure: The impact of Na leaching', *Cement and Concrete Research*, 178, p. 107432. Available at: https://doi.org/10.1016/j.cemconres.2024.107432.

Liu, H. *et al.* (2021) 'Coupling effect of steel slag in preparation of calcium-containing geopolymers with spent fluid catalytic cracking (FCC) catalyst', *Construction and Building Materials*, 290, p. 123194. Available at: https://doi.org/10.1016/j.conbuildmat.2021.123194.

Liu, J. *et al.* (2021) 'Hierarchically porous covalent organic framework for adsorption and removal of triphenylmethane dyes', *Microporous and Mesoporous Materials*, 312, p. 110703. Available at: https://doi.org/10.1016/j.micromeso.2020.110703.

Liu, X. *et al.* (2022) 'Carbonation behavior of calcium silicate hydrate (C-S-H): Its potential for CO2 capture', *Chemical Engineering Journal*, 431, p. 134243. Available at: https://doi.org/10.1016/j.cej.2021.134243.

Liu, Z. *et al.* (2019) 'Microstructure and phase evolution of alkali-activated steel slag during early age', *Construction and Building Materials*, 204, pp. 158–165. Available at:

https://doi.org/10.1016/j.conbuildmat.2019.01.213.

Ma, L. *et al.* (2024) 'A sustainable carbon aerogel from waste paper with exceptional performance for antibiotics removal from water', *Journal of Hazardous Materials*, 474, p. 134738. Available at: https://doi.org/10.1016/j.jhazmat.2024.134738.

Mahardiani, L. *et al.* (2021) 'Nanocellulose Obtained from Biomass as Advance Adsorbent for Methylene Blue and Crystal Violet', *Journal of Physics: Conference Series*, 1912(1), p. 012015. Available at: https://doi.org/10.1088/1742-6596/1912/1/012015.

Maleki, A. *et al.* (2020) 'Adsorbent materials based on a geopolymer paste for dye removal from aqueous solutions', *Arabian Journal of Chemistry*, 13(1), pp. 3017–3025. Available at: https://doi.org/10.1016/j.arabjc.2018.08.011.

Matalkah, F. and Soroushian, P. (2023) 'Role of CO2 in enhancing geopolymer properties formulated with fluidized bed combustion ash', *Journal of CO2 Utilization*, 71, p. 102462. Available at: https://doi.org/10.1016/j.jcou.2023.102462.

Menges, F. (no date) 'F. Menges "Spectragryph - optical spectroscopy software", Version 1.2.16.1, 2022, http://www.effemm2.de/spectragryph/'.

Mushtaq, M. *et al.* (2016) 'Eriobotrya japonica seed biocomposite efficiency for copper adsorption: Isotherms, kinetics, thermodynamic and desorption studies', *Journal of Environmental Management*, 176, pp. 21–33. Available at: https://doi.org/10.1016/j.jenvman.2016.03.013.

Mužek, M.N., Svilović, S. and Zelić, J. (2014) 'Fly ash-based geopolymeric adsorbent for copper ion removal from wastewater', *Desalination and Water Treatment*, 52(13–15), pp. 2519–2526. Available at: https://doi.org/10.1080/19443994.2013.792015.

Nobouassia Bewa, C. *et al.* (2018) 'Water resistance and thermal behavior of metakaolin-phosphate-based geopolymer cements', *Journal of Asian Ceramic Societies*, 6(3), pp. 271–283. Available at: https://doi.org/10.1080/21870764.2018.1507660.

Nuñez, O. *et al.* (2019) 'Synthesis and DNA binding profile of monomeric, dimeric, and trimeric derivatives of crystal violet', *Bioorganic Chemistry*, 83, pp. 297–302. Available at: https://doi.org/10.1016/j.bioorg.2018.10.040.

Phoo-ngernkham, T. *et al.* (2015) 'Effects of sodium hydroxide and sodium silicate solutions on compressive and shear bond strengths of FA–GBFS geopolymer', *Construction and Building Materials*, 91, pp. 1–8. Available at: https://doi.org/10.1016/j.conbuildmat.2015.05.001.

Raghu, S. and Ahmed Basha, C. (2007) 'Chemical or electrochemical techniques, followed by ion exchange, for recycle of textile dye wastewater', *Journal of Hazardous Materials*, 149(2), pp. 324–330. Available at: https://doi.org/10.1016/j.jhazmat.2007.03.087.

Rajerajesw, A., Dhinakaran, G. and Ershad, M. (2014) 'Compressive Strength of Silica Fume Based Geopolymer Concrete', *Asian Journal of Applied Sciences*, 7(4), pp. 240–247. Available at: https://doi.org/10.3923/ajaps.2014.240.247.

Rojas, J. *et al.* (2019) 'Kinetics, Isotherms and Thermodynamic Modeling of Liquid Phase Adsorption of Crystal Violet Dye onto Shrimp-Waste in Its Raw, Pyrolyzed Material and Activated Charcoals', *Applied Sciences*, 9(24), p. 5337. Available at: https://doi.org/10.3390/app9245337.

Roy, D.C. *et al.* (2018) 'Biodegradation of Crystal Violet dye by bacteria isolated from textile industry effluents', *PeerJ*, 6, p. e5015. Available at: https://doi.org/10.7717/peerj.5015.

Salimi, M. and Ghorbani, A. (2020) 'Mechanical and compressibility characteristics of a soft clay stabilized by slag-based mixtures and geopolymers', *Applied Clay Science*, 184, p. 105390. Available at:

https://doi.org/10.1016/j.clay.2019.105390.

Sarma, J. and Mahiuddin, S. (2014) 'Specific ion effect on the point of zero charge of α-alumina and on the adsorption of 3,4-dihydroxybenzoic acid onto α-alumina surface', *Colloids and Surfaces A: Physicochemical and Engineering Aspects*, 457, pp. 419–424. Available at: https://doi.org/10.1016/j.colsurfa.2014.06.014.

Silva, C.A.R.D. *et al.* (2002) 'Carbonation-Related Microstructural Changesin Long-Term Durability Concrete', *Materials Research*, 5(3), pp. 287–293. Available at: https://doi.org/10.1590/S1516-14392002000300012.

Singh, N.B. (2020) 'Properties of cement and concrete in presence of nanomaterials', in *Smart Nanoconcretes and Cement-Based Materials*. Elsevier, pp. 9–39. Available at: https://doi.org/10.1016/B978-0-12-817854-6.00002-7.

Singh, N.B. and Middendorf, B. (2020) 'Geopolymers as an alternative to Portland cement: An overview', *Construction and Building Materials*, 237, p. 117455. Available at: https://doi.org/10.1016/j.conbuildmat.2019.117455.

Singh, S.P., Tripathy, D.P. and Ranjith, P.G. (2008) 'Performance evaluation of cement stabilized fly ash–GBFS mixes as a highway construction material', *Waste Management*, 28(8), pp. 1331–1337. Available at: https://doi.org/10.1016/j.wasman.2007.09.017.

Siyal, A.A. *et al.* (2018) 'A review on geopolymers as emerging materials for the adsorption of heavy metals and dyes', *Journal of Environmental Management*, 224, pp. 327–339. Available at: https://doi.org/10.1016/j.jenvman.2018.07.046.

Sun, S. *et al.* (2023) 'Adsorption of crystal violet on activated bamboo fiber powder from water: preparation, characterization, kinetics and isotherms', *RSC Advances*, 13(9), pp. 6108–6123. Available at: https://doi.org/10.1039/D2RA08323J.

T., S. *et al.* (2022) 'A state-of-the-art on development of geopolymer concrete and its field applications', *Case Studies in Construction Materials*, 16, p. e00812. Available at: https://doi.org/10.1016/j.cscm.2021.e00812.

Trinh, T.T.P.N.X. *et al.* (2021) 'Preparing three-dimensional graphene aerogels by chemical reducing method: Investigation of synthesis condition and optimization of adsorption capacity of organic dye', *Surfaces and Interfaces*, 23, p. 101023. Available at: https://doi.org/10.1016/j.surfin.2021.101023.

Vithalkar, S.H. and Jugade, R.M. (2020) 'Adsorptive removal of crystal violet from aqueous solution by cross-linked chitosan coated bentonite', *Materials Today: Proceedings*, 29, pp. 1025–1032. Available at: https://doi.org/10.1016/j.matpr.2020.04.705.

Wang, J. and Guo, X. (2020) 'Adsorption isotherm models: Classification, physical meaning, application and solving method', *Chemosphere*, 258, p. 127279. Available at: https://doi.org/10.1016/j.chemosphere.2020.127279.

Wathukarage, A. *et al.* (2019) 'Mechanistic understanding of crystal violet dye sorption by woody biochar: implications for wastewater treatment', *Environmental Geochemistry and Health*, 41(4), pp. 1647–1661. Available at: https://doi.org/10.1007/s10653-017-0013-8.

Wei, Y. *et al.* (2020) 'Hydrothermal processing, characterization and leaching toxicity of Cr-added "fly ash-metakaolin" based geopolymer', *Construction and Building Materials*, 251, p. 118931. Available at: https://doi.org/10.1016/j.conbuildmat.2020.118931.

Xu, D. (2008) 'Adsorption of Pb(II) from aqueous solution to MX-80 bentonite: Effect of pH, ionic strength, foreign ions and temperature', *Applied Clay Science*, 41(1–2), pp. 37–46. Available at: https://doi.org/10.1016/j.clay.2007.09.004.

Yao, Z.-Y., Qi, J.-H. and Wang, L.-H. (2010) 'Equilibrium, kinetic and thermodynamic studies on the biosorption of Cu(II) onto chestnut shell', *Journal of Hazardous Materials*, 174(1–3), pp. 137–143. Available at:

https://doi.org/10.1016/j.jhazmat.2009.09.027.

Zhang, H. *et al.* (2010) 'Electrochemical oxidation of Crystal Violet in the presence of hydrogen peroxide', *Journal of Chemical Technology & Biotechnology*, 85(11), pp. 1436–1444. Available at: https://doi.org/10.1002/jctb.2447.

Zhang, L. *et al.* (2024) 'Synergistic effect and reinforcement mechanism of porous inorganic polymers via the fiber addition and carbonation curing', *Journal of Building Engineering*, 92, p. 109743. Available at: https://doi.org/10.1016/j.jobe.2024.109743.

Zhang, Y. *et al.* (2022) 'Full process of calcium silicate hydrate decalcification: Molecular structure, dynamics, and mechanical properties', *Cement and Concrete Research*, 161, p. 106964. Available at: https://doi.org/10.1016/j.cemconres.2022.106964.

Zhou, J., Ma, F. and Guo, H. (2020) 'Adsorption behavior of tetracycline from aqueous solution on ferroferric oxide nanoparticles assisted powdered activated carbon', *Chemical Engineering Journal*, 384, p. 123290. Available at: https://doi.org/10.1016/j.cej.2019.123290.